PAPER

Check for updates

Elucidating the geometric and electronic structure of a fully sulfided analog of an Anderson polyoxomolybdate cluster

S. M. Gulam Rabbani,[a] Zhihengyu Chen,[b] Jingyi Sui,[c] Joseph T. Hupp, [ID][c]
Karena W. Chapman[b] and Rachel B. Getman [ID] [a]

The catalytic activity of transition metal sulfide (TMS) clusters in small molecule activation, redox transformations, and charge transfer has inspired the design of novel TMS-based materials for energy-related catalysis and chemical applications. Polyoxometalates (POMs), known for their structural diversity, can in principle be transformed into TMS clusters; however, fully sulfided analogs are rarely isolated, likely due to the strong tendency of uncapped TMS clusters to agglomerate. Here, we report the geometric and electronic structure of a capping ligand-free fully sulfided analog of heptamolybdate Anderson POM $[Mo^{VI}_7O_{24}]^{6-}$, synthesized through the sulfidation of a nanoconfined POM secured within a porous Zr-metal organic framework (NU-1000). A combined computational and experimental analysis indicates that the sulfided counterpart of the Anderson POM is geometrically and electronically more sophisticated than the parent POM. Comparison of experimental pair distribution function (PDF) data with computational simulations confirms that, unlike the oxygen-only $[Mo^{VI}_7O_{24}]^{6-}$ cluster, the $[Mo^{IV}_7(\mu_3\text{-}S)_6(\mu_2\text{-}SH)_6(S_2)_6]^{2-}$ polythiometalate (PTM) exhibits diverse sulfur anions (S^{2-}, HS^-, S_2^{2-}). DFT calculations indicate that H_2S acts as a reducing agent, and together with terminal disulfide (S_2^{2-}) ligands in the PTM structure, facilitates the complete reduction of all seven Mo^{VI} centers in the parent POM to Mo^{IV}. These findings are supported by X-ray photoelectron spectroscopy (XPS), which confirms exclusive Mo^{IV}, and elemental analysis, which shows quantitative sulfur incorporation. Difference envelope density (DED) mapping further reveals that the PTM clusters are spatially confined within the MOF pores, preventing agglomeration and preserving molecular integrity.
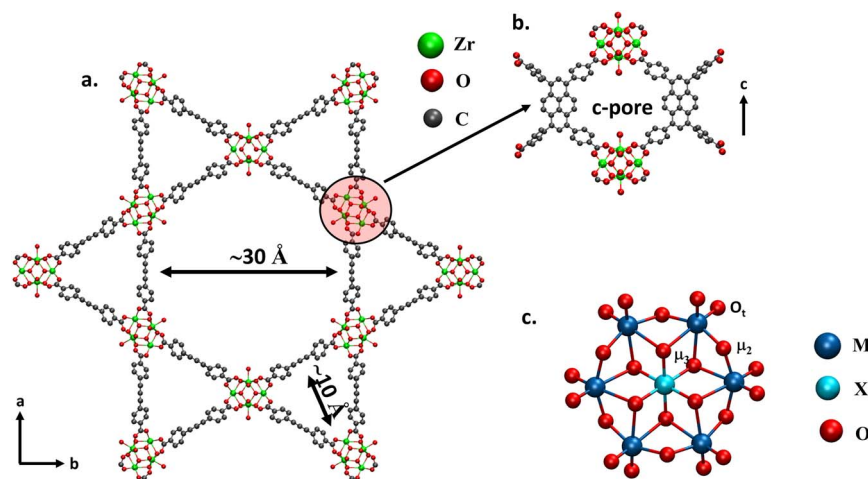
Introduction

Transition metal sulfide (TMS) clusters are versatile platforms for sustainable energy catalysis, owing to their rich structural diversity, flexible redox chemistry, and dynamic charge-transfer capabilities.[1–5] Inspired in part by their biological counterparts—which mediate multi-electron bond activations in nitrogenases,[6–8] nitrous oxide reductase,[9] and carbon monoxide dehydrogenases[10–13]—synthetic TMS clusters have been explored as molecular models and functional catalysts for hydrogen evolution, CO_2 reduction, and other reductive transformations.[14–17] Among metal oxides, polyoxometalates (POMs)—particularly those composed of Mo, W, or V in high oxidation states—offer precise structural control and electronic versatility, making them appealing precursors for sulfided

analogs.[18–20] In theory, substituting sulfur for oxygen in well-defined polyoxometalate (POM) structures should yield a wide variety of polythiometalates (PTMs); however, reports of fully sulfided POM analogs are scarce.[21] This scarcity could be attributed to the strong internal metal-sulfur redox reactions and the tendency of uncapped PTMs to agglomerate.[22–24]

We have recently shown that capping-ligand-free, fully sulfided analogs of the well-defined Anderson polyoxometalate $[Co^{III}Mo^{VI}_6O_{24}]^{3-}$ can be accessed by sulfidating the POM precursor when immobilized within the Zr-metal organic framework NU-1000 (MOFkey:[25] Zr.HVCDAMXLLUJLQZ.MOFkey-v1.csq; see Fig. 1a).[25–27] In NU-1000, the reactant-accessible c pore (Fig. 1b) spatially separates and confines the POMs (Fig. 1c), enabling controlled sulfidation within these confined microenvironments. A difference envelope density (DED) map reveals that, like the POM precursors, the resulting PTMs are individually isolated within the open-channel-connected micropores of the MOF, thereby preventing their agglomeration. Assessments of elemental composition establish that the replacement of the oxygen ions of each POM by sulfur ions is quantitative within experimental uncertainty. No evidence for loss of Mo or Co is observed.

[a]William G. Lowrie Department of Chemical and Biomolecular Engineering, The Ohio State University, Columbus, Ohio 43210, USA. E-mail: getman.11@osu.edu

[b]Department of Chemistry, Stony Brook University, Stony Brook, New York 11794, USA. E-mail: karena.chapman@stonybrook.edu

[c]Department of Chemistry, Northwestern University, Evanston, Illinois 60208, USA. E-mail: j-hupp@northwestern.edu

32382 | *J. Mater. Chem. A*, 2025, **13**, 32382–32390

This journal is © The Royal Society of Chemistry 2025

Fig. 1 (a) Crystal structure of NU-1000, showing 30 and 10 Å channels along the *c*-axis, (b) side view of the c pore, (c) top views of an α-type planar Anderson POM, which can be anchored in the c pore. X represents a heterometal center. Hydrogen atoms in a, b, and c are omitted for clarity.

Further, XPS measurements indicate complete conversion of Mo^{VI} to Mo^{IV}, which is supported by density functional theory (DFT) calculations.

Preliminary results indicate that PTM@MOF materials remain structurally stable up to 300–350 °C under hydrogenation conditions. However, sensitized framework photolysis experiments revealed that $Mo_6CoS_{24}^{m-}$@NU-1000, as initially synthesized, is catalytically inactive for evolution of molecular hydrogen from an acidified mixture of acetonitrile and water. With extended photolysis, however, the MOF-immobilized cluster became progressively more catalytic. Concomitant with increasing activity is loss of sulfur and release of H_2S. The behavior was tentatively attributed to progressively increasing exposure of otherwise coordinatively saturated molybdenum centers to potentially reactive hydronium ions. The stability of these materials when isolated in NU-1000, as well as their promise for thermal- and electrocatalytic reduction motivates this study into the PTM composition and structure.

Unlike bulk or 2D MoS_2, where only edge sites are active and basal planes remain inert,[28–30] Anderson-type PTMs expose nearly all Mo and S atoms, yielding a high density of catalytic sites that enhance activity and facilitate molecular-level structure-activity studies. All-molybdenum sulfide clusters additionally offer a compositionally uniform and structurally simplified platform for probing how sulfur coordination and molybdenum reduction influence redox behavior—insights often obscured in heterometallic or amorphous systems. Low-nuclearity thiomolybdates such as $[Mo_3S_{13}]^{2-}$ and $[Mo_2S_{12}]^{2-}$ have served as useful molecular models for catalytically active MoS_x motifs,[4,31,32] but their limited nuclearity restricts the degree of structural complexity and electronic delocalization they can capture. In contrast, higher-nuclearity clusters such as Mo_7S_{24} may overcome these limitations by combining the tunable electronic properties of molecular systems with local geometric features resembling amorphous MoS_x.[33–35] If these structural and electronic parallels are confirmed, the clusters can serve as atomically precise models for probing the factors that govern redox catalysis, ultimately guiding the design of PTMs and molybdenum sulfides for hydrogen evolution and other reductive transformations.

Along these lines, in this manuscript, we combined computational and experimental methods to study the geometric and electronic structure of the sulfided analog of a heptamolybdate Anderson POM $[Mo^{VI}_7O_{24}]^{6-}$. Our objective was to shed light on: (i) what geometrical structural features uniquely differentiate the PTM from the parent POM, and (ii) how does wholesale replacement of oxygen by sulfur change the cluster electronic structure? Inductively coupled plasma optical emission spectroscopy (ICP-OES), X-ray photoelectron spectroscopy (XPS), pair distribution function (PDF) analysis, and DED mapping were employed to probe elemental composition, oxidation states, local coordination environments, and spatial confinement—revealing the expected stoichiometry, complete reduction of Mo^{VI} to Mo^{IV}, diverse sulfur ligands, and discrete localization within the MOF pores. Extensive DFT calculations refine the structural model to a Mo_7S_{24} core composed of S^{2-}, HS^-, and S_2^{2-} ligands, indicating that H_2S acts as both sulfur source and reducing agent, facilitating Mo reduction *via* terminal disulfide formation. This wholesale sulfur substitution preserves the cluster's compact geometry while significantly modulating its frontier orbitals, resulting in a delocalized, redox-active electronic structure consistent with enhanced catalytic performance.

Synthesis details

NU-1000 was synthesized according to the literature.[36] Mo_7S_{24}@NU-1000 was synthesized as follows. Ammonium molybdate tetrahydrate (60 mg, 0.049 mmol) was dissolved in 10 mL of deionized water. NU-1000 (50 mg, 0.023 mmol) was added to the solution and dispersed by sonication for about 1 minute. The suspension was shaken periodically. After 3 days, the solid was washed three times with water and soaked in acetone overnight. Then, the solid was washed two more times

This journal is © The Royal Society of Chemistry 2025

J. Mater. Chem. A, 2025, **13**, 32382–32390 | **32383**

with acetone and dried at 80 °C for 4 h under vacuum prior to activation on the Smart VacPrep. The dried sample (50 mg) was placed in a tube furnace and subjected to 25 sccm of 4%H_2S/N_2, and the temperature was increased at a rate of 5 °C min^{-1} to 180 °C. After 18 h, the sample was cooled to room temperature under N_2 and stored under inert environments.

Additional experimental methods

ICP-OES, XPS, powder X-ray diffraction (PXRD) with DED analysis, and PDF analysis and methods are detailed in SI Section 1.

Computational details

Geometries of all studied structures were optimized in the gas phase without any geometric constraints using DFT as implemented in the Gaussian16 code.[37] The M06-L functional[38] was employed. The molybdenum center was described using the def2-TZVPP basis set, while all the other centers were described using the def2-SVP basis set.[39,40] Default convergence criteria were used in electronic structure and geometry relaxations. Computation of vibrational frequencies confirmed all structures to be minima on the potential energy surface. Molecular orbitals and band gaps were calculated through single-point calculations using the hybrid MN15 functional[42] and Def2TZVPP basis set on the optimized structures using the method described above. This functional was used for these calculations since hybrid functionals with the incorporation of fractions of the exact Hartree–Fock exchange perform better for computing precise electronic structures. Gibbs free energies were calculated at 298.15 K and 1.0 atm. The procedure for identifying PTM species with varying hydrogen contents is detailed in SI Section 2.1. Some PTM clusters considered for the DFT calculations contained reduced Mo centers, which have the possibility of multiple spin multiplicities. Testing of the $[Mo_7S_{18}(SH)_6]$ species revealed that low-spin states are more electronically favorable than high-spin states (see Table S1). Therefore, while searching for isomers with varying H content, we only considered the lowest spin state. However, once we identified the favorable isomers, we computed multiple spin states and noticed that even these species favored low spin states (see Table S2).

In this study, gas-phase modeling was employed to gain a fundamental understanding of the intrinsic structural and electronic properties of the cluster. This approach is consistent with the structural characteristics observed in experimental analyses and reflects the conditions under which the cluster was synthesized. While we acknowledge that solvent effects can influence the electronic structure and reactivity of molecular clusters—particularly in solvated environments—reactivity modeling is beyond the scope of the present work. Nevertheless, solvent effects will be considered in a follow-up study focused on cluster reactivity in solutions. Additionally, we evaluated the spin multiplicity of the final $[Mo_7S_{18}(SH)_6]^{2-}$ (**b-H_6^{2-}**) structure in both the gas phase and in acetonitrile solvent using the SMD implicit solvation model.[41] Results are shown in Table S2. They indicate that low-spin states are energetically favored in both

cases, suggesting that spin-state preferences are consistent across gas and solvent environments.

Results

Experimental results

Following the synthesis of the fully sulfided polyoxomolybdate (PTM) cluster within the NU-1000 MOF, we carried out comprehensive characterization to elucidate its geometric and electronic features. ICP-OES was performed on the synthesized material to learn the relative S to Mo composition. This data showed that the S/Mo ratio is 3.87. XPS was employed to provide additional data, as well as to learn the oxidation states of the Mo centers. The S scan of XPS showed no sulfate, indicating that all oxygen within the POM were replaced with sulfur during the synthesis of the PTM cluster.

XPS also indicated that the oxidation state of the molybdenum centers in the synthesized PTM was significantly different than the parent Anderson POM. For example, the Mo 3d spectrum (Fig. 2b) consisted of peaks at approximately 229 eV and 233 eV, which correspond to the $3d_{5/2}$ and $3d_{3/2}$ components of Mo^{IV} in the PTM, whereas only the Mo^{VI} is present in the parent POM. The broad S 2s feature observed near the Mo $3d_{5/2}$ peak indicates the presence of sulfur in multiple forms. In contrast, in the parent POM the corresponding oxygens are present only as monoatomic, proton-free dianions (albeit, in both terminal and bridging configurations). For further analysis, we examined the S 2p region of the PTM, which was fitted with two distinct doublets ($2p_{3/2}$, $2p_{1/2}$; Fig. 2c). XPS data indicated a higher binding energy doublet at 163.8 and 164.9 eV, reflecting the presence of bridging sulfhydryl (SH^-) and apical S^{2-} ligands, along with a lower binding energy doublet at 162.3 and 163.5 eV, attributed to terminal S_2^{2-} ligands.[31,43] Thus, the PTM contains sulfur atoms (sulfide and sulfhydryl) having a formal oxidation state of –II as well sulfur atoms (disulfide atoms) having a formal oxidation state of –I. The formation of S_2^{2-} from H_2S (i.e., sulfur in oxidation state –II) points to H_2S as a source of reducing equivalents for the conversion of Mo^{VI} to Mo^{IV}.

Powder X-ray diffraction (PXRD) data for PTM@NU-1000 (Fig. S7) exhibit a slight increase in low-angle diffuse scattering compared to the POM-loaded starting material, which may suggest structural disorder introduced during sulfidation or the presence of a second non-periodic phase. To assess the location and verify the isolated nature of the clusters, difference envelope density (DED) analysis was carried out based on synchrotron X-ray scattering data. DED analysis, obtained by subtracting the structure envelope of pristine NU-1000 from that of POM@NU-1000 and PTM@NU-1000, revealed that both the parent Anderson POM and its fully sulfided analog are localized in the NU-1000 c-pore, with partial extension towards the adjacent triangular channels (Fig. 2a and S6). As we have shown for related systems, nanoscale confinement is crucial for suppressing agglomeration,[44,45] a common issue for uncapped or unsupported PTMs. By physically isolating the clusters, NU-1000 stabilizes discrete, well-defined molecular species and prevents their transformation into disordered or amorphous aggregates.
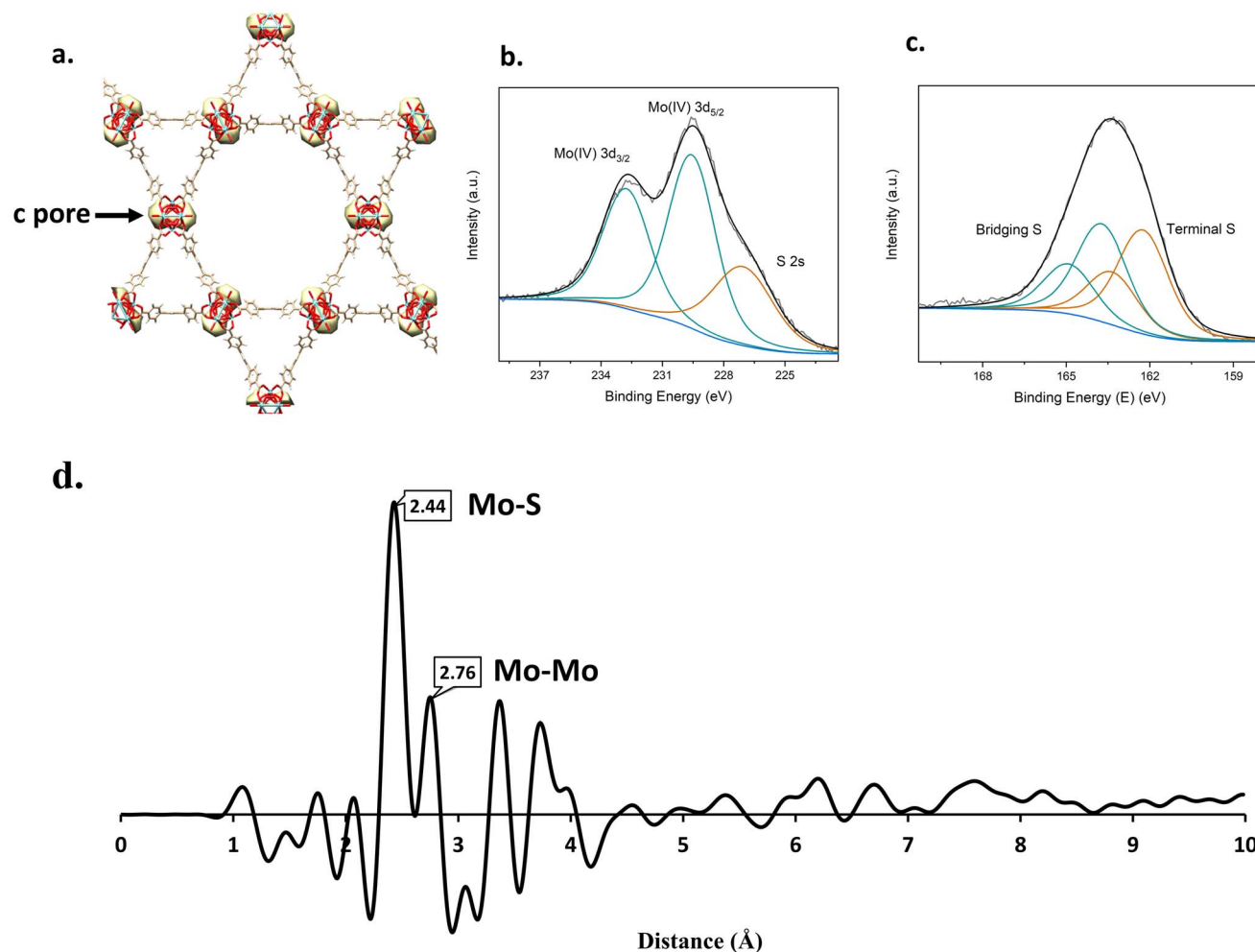
32384 | J. Mater. Chem. A, 2025, 13, 32382–32390

This journal is © The Royal Society of Chemistry 2025

Fig. 2 (a) Difference envelope density plot corresponding to the location of the PTM (yellow surface) in the NU-1000 c pore. (b) and (c) X-ray photoelectron spectra of the Mo 3d (b) and S 2p regions (c). (d) Differential pair distribution function data obtained for the PTM@NU-1000 system.

Differential PDF (d-PDF; Fig. 2d) was carried out to interrogate the PTM structure. The d-PDF of the parent $[Mo^{VI}_7O_{24}]^{6-}$ cluster is included in the SI Section 3 for reference. d-PDF results were obtained by subtracting the PDF for pristine NU-1000 from that of the PTM@NU-1000. Results from d-PDF illustrate the closest Mo–S and Mo···Mo distances (*i.e.*, low *r* region; the dash and ellipsis indicate directly and indirectly connected atom pairs, respectively) within the PTM. Specifically, the well-defined peaks at ~2.44 Å and at 2.76 Å correspond to the Mo–S and Mo···Mo distances within the PTM. At longer distances, where there are multiple discrete atom–atom correlations of similar distance, the assignment of peaks in the PDF to specific atom–atom pairs is less straightforward. The features in the d-PDF associated with the PTM clusters confined within NU-1000 are distinctly different than observed in previous PDF studies of amorphous MoS_x phases.[46] Indeed, the sharp Mo–S and Mo···Mo correlations observed in the d-PDF for the PTM confirm a well-defined local structure. The absence of features beyond ~5 Å in the d-PDF suggests that this order is confined to a molecular scale, as is consistent with a discrete cluster. Collectively, the PDF, PXRD, and DED analyses all indicate that

the PTM forms a locally ordered, discrete molecular cluster that is spatially confined within the c-pores of NU-1000. These findings also confirm significant structural transformation and full reduction of Mo centers from Mo^{VI} to Mo^{IV}. Nevertheless, precise structural assignment and a deeper understanding of the electronic structure necessitate computational modeling, which is described in the following section.

Computational results

The results from the XPS study, which identified reduced Mo centers and a variety of sulfur-based ligands in the synthesized PTM, provide a basis for modeling the geometric structure of the PTM. Based on these results, we constructed four possible model structures with the chemical composition of $[Mo_7S_{24}]^{6-}$. These structures are shown in Fig. 3 and are labeled **a**, **b**, **c**, and **d**. Structure **a** is the exact analog of the Anderson POM built by replacing O with S. Structures **a**, **b**, **c**, and **d** exhibit various types of sulfide groups such as bridging sulfides/disulfides (S^{2-}/S_2^{2-}), terminal sulfides/disulfides (S^{2-}/S_2^{2-}), and apical sulfides (μ_3-S^{2-}), which have also been observed in the structures of other thiomolybdates.[2,47–49] Structures **a**, **b**, and **c** have the same
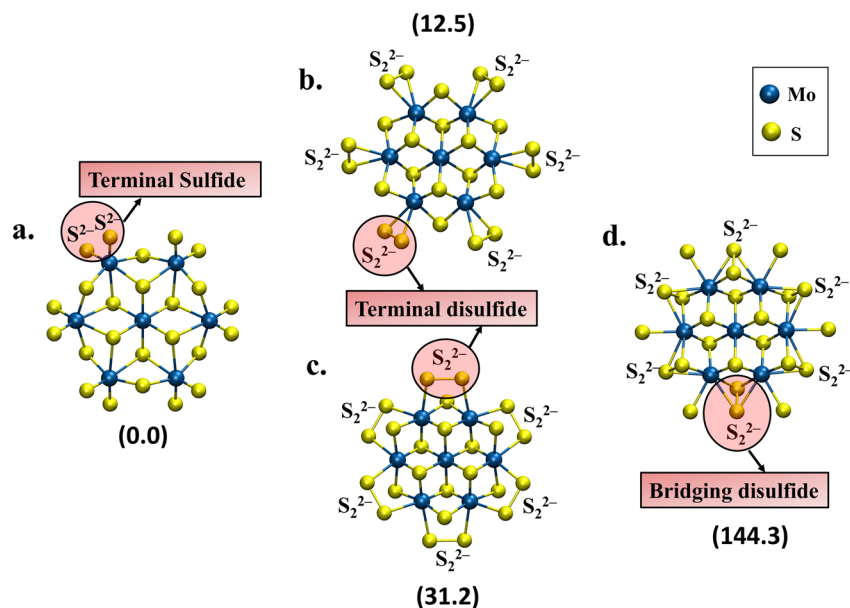
This journal is © The Royal Society of Chemistry 2025

J. Mater. Chem. A, 2025, **13**, 32382–32390 | **32385**

Fig. 3 (a–d) Possible structures considered for modeling the sulfided analog of Anderson polyoxometalate $[Mo^{VI}_7O_{24}]^{6-}$ and their relative Gibbs free energies (in parentheses) at standard state in units of kcal mol^{-1}. Structures a, b, c, and d have the same labels as in the text.
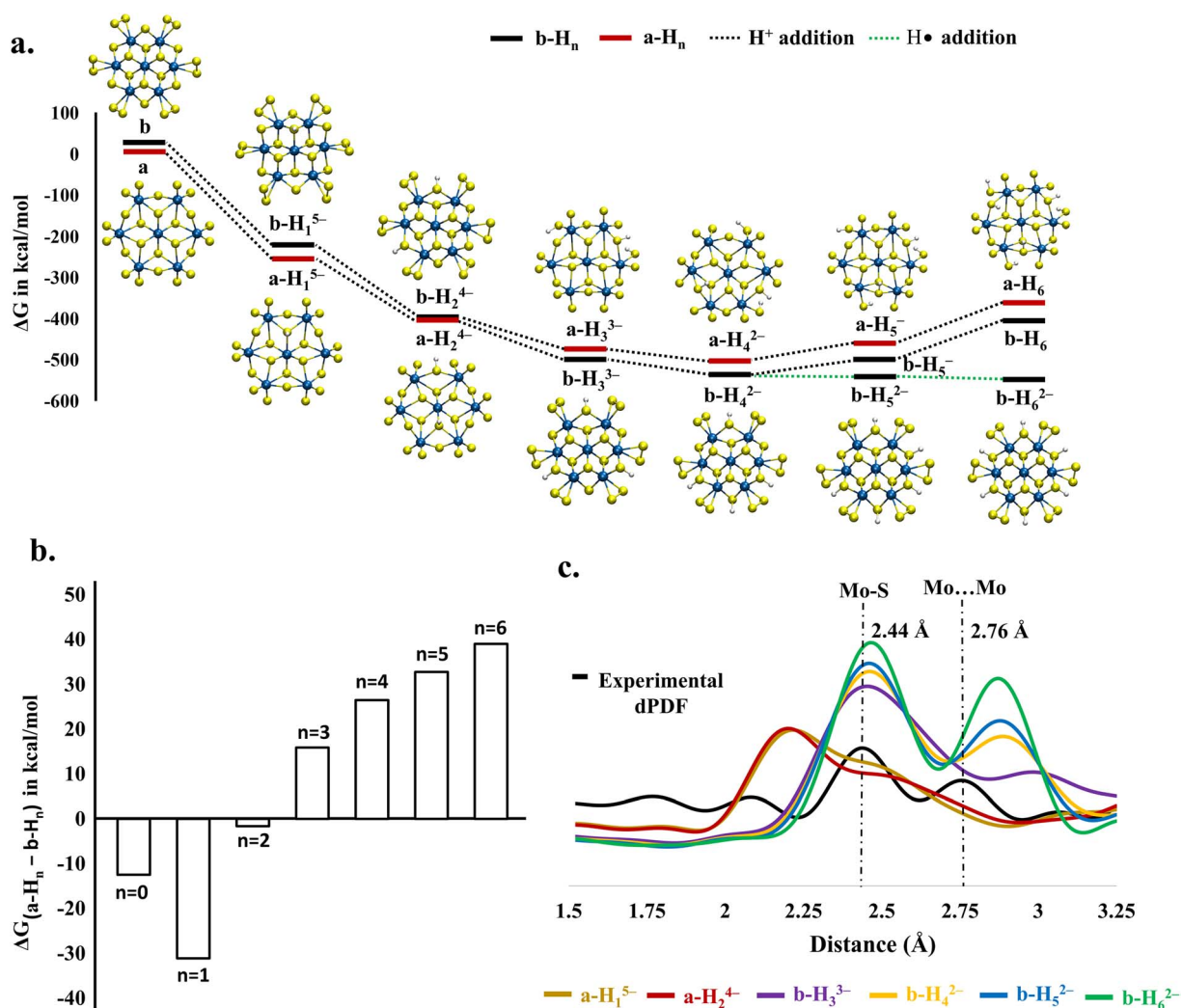

Fig. 4 (a) Thermodynamically favorable isomers of $a\text{-}H_n$ and $b\text{-}H_n$ species with increasing hydrogen content (n). Hydrogen can be added as protons (H^+) or atoms ($H^\bullet$). (b) ΔG calculated as $G_{a\text{-}H_n} - G_{b\text{-}H_n}$ in units of kcal mol^{-1} for $n = 0$ to 6. (c) d-PDFs for the synthesized structure (in black) and simulated structures (in colors).

32386 | J. Mater. Chem. A, 2025, 13, 32382–32390

This journal is © The Royal Society of Chemistry 2025

$Mo_7(\mu_3\text{-}S)_6(\mu_2\text{-}S)_6$ core, whereas structure **d** has a core containing six bridging disulfides. Further, structures **b**, **c**, and **d** have six disulfides, resulting in reduced Mo centers, while **a** has 12 terminal sulfides, resulting in fully oxidized Mo^{VI} centers—notably at odds with the experimental finding of molybdenum exclusively in oxidation state IV.

All model structures have the same $[Mo_7S_{24}]^{6-}$ chemical composition, which allows thermodynamic stability comparison. Structure **a**, which resembles the structure of the parent POM, is thermodynamically the most favorable structure, while structure **d**, which comprises bridging disulfide ligands (S_2^{2-}) is the most unfavorable structure with a relative free energy of 144.3 kcal mol^{-1}. This suggests that bridging disulfide ligands are very unstable in these PTMs. Among the clusters containing terminal disulfide ligands (S_2^{2-}), structure **b** is more favorable than **c**, making it the 2nd most favorable geometric configuration amongst the model structures. The terminal disulfide ligands (S_2^{2-}) in **b** are connected to one molybdenum center as commonly observed in thiomolybdates.

Since structure **a** is thermodynamically most favorable, we computed the thermodynamics of the generation of this PTM species due to the reaction of the $[Mo_7O_{24}]^{6-}$ POM with H_2S, forming H_2O (see SI Fig. S1a). We find this reaction is endergonic by 25.0 kcal mol^{-1}. On the other hand, the presence of protons in the cluster stabilizes the PTM, making the sulfidation of the POM thermodynamically viable (Fig. S1b). Therefore, we considered the thermodynamics of PTM formation with various numbers of added protons. Since structures **a** and **b** were found to be the most stable, we explored the protonation of both clusters by adding up to 6 protons to each structure (Fig. 4a). Protonation suggests that the sulfided analog of the Anderson POM contains sulfhydryl (SH^-) groups, which is in contrast to the Anderson POM which lacks hydroxyl groups (OH^-). Multiple proton configurations were evaluated to find the most stable isomer, since various sulfur atoms could potentially be protonated. Fig. 4a shows the thermodynamically most favorable isomers with addition of up to 6 protons. The energies of other isomers are available in SI Tables S3 and S4. Fig. 4b shows that the thermodynamic stability trend of $\textbf{a-H}_n$ and $\textbf{b-H}_n$ species depends on the number (n) of protons present. For values of n between 0 and 2, $\textbf{a-H}_n$ structures are more favorable. However, for $2 < n \leq 6$, $\textbf{b-H}_n$ structures become more favorable. The structural stability, hence, depends on the proton content.

Next, we employed PDF analysis in order to compare with the synthesized structure. PDFs of the simulated structures (colored lines) are compared with the experimental d-PDF (black line) in Fig. 4c. Since most peaks found in the experimental d-PDF are located between 1.5 to 4 Å (Fig. 2d, and 4c), Pearson correlation analysis between the simulated ($\textbf{a-H}_n$, $\textbf{b-H}_n$, **c**, and **d**) and experimental structures was performed in that range. Further details about this analysis are provided in SI Fig. S4. In general, $\textbf{b-H}_n$ species have higher average Pearson correlation coefficients (0.49) with the experimental structure than $\textbf{a-H}_n$ species (0.29), indicating that the synthesized PTM has more structural similarities with $\textbf{b-H}_n$ structures. We additionally compared distances (Mo–S and Mo···Mo) in the favorable protonated PTM

structures (from Fig. 4a) with the experimental d-PDF Mo–S and Mo···Mo distances of ∼2.44 Å and 2.76 Å. The first two intense peaks in the simulated $\textbf{b-H}_n$ structures (purple, yellow, blue, and green lines in Fig. 4c) are Mo–S at ∼2.45 Å and Mo···Mo at ∼2.88 Å, which are similar to the experimental dPDF. Conversely, $\textbf{a-H}_n$ structures (gold and red in Fig. 4c) display a single peak for Mo–S at ∼2.20 Å, which is shorter than that observed in experimental dPDF. Further, $\textbf{a-H}_n$ structures exhibit no Mo···Mo peak due to longer Mo···Mo distances in the $\textbf{a-H}_n$ structures. Therefore, the Pearson correlation and consideration of Mo–S and Mo···Mo bond distances indicate that $\textbf{b-H}_n$ species are structurally more similar to the experimental structure than proposed $\textbf{a-H}_n$ structures. This finding is consistent with XPS results which indicate the presence of reduced Mo centers. We discuss below that the reduced centers result from the conversion of multiple sulfides (S^{2-}; oxidation state of –II) to terminal disulfide ligands (S_2^{2-}; with oxidation state of –I) due to exposure to H_2S. These findings are additionally consistent with free energy calculations, which show that for $2 < n \leq 6$, $\textbf{b-H}_n$ structures are more stable than $\textbf{a-H}_n$ structures, and that the addition of up to four protons to either species remains thermodynamically favorable.

The addition of a 5th proton (H^+) is thermodynamically disfavored by 31.5 kcal mol^{-1} (Fig. 4a); however, the hydrogen content of the $\textbf{b-H}_4^{2-}$ cluster can be increased using a reducing agent such as H_2S which is present in PTM synthesis. Under H_2S, two hydrogen atoms ($H\cdot$) can be added to the $\textbf{b-H}_4^{2-}$ cluster, resulting in the formation of $\textbf{b-H}_6^{2-}$ (Fig. 4a). Further reduction of the $\textbf{b-H}_6^{2-}$ PTM by H_2S will further change the oxidation state of Mo in the PTM. Protonation of $\textbf{b-H}_6^{2-}$ to form $\textbf{b-H}_7^-$ is unfavorable by 37.6 kcal mol^{-1} (Fig. S3); therefore, the $\textbf{b-H}_6^{2-}$ species is the thermodynamically most feasible model.
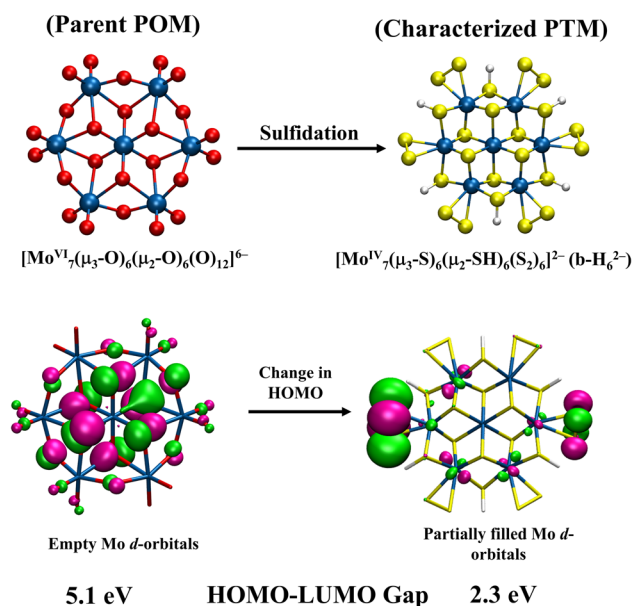

Fig. 5 Structure (top) and highest occupied molecular orbital (isovalue = 0.03; bottom) of the Anderson POM (left) and the characterized PTM (right). The PTM orbital uses the triplet structure which is nearly iso-energetic to the singlet (low spin) structure for visual purposes.

(Parent POM)   **(Characterized PTM)**

Sulfidation

$[Mo^{VI}_7(\mu_3\text{-}O)_6(\mu_2\text{-}O)_6(O)_{12}]^{6-}$ $[Mo^{IV}_7(\mu_3\text{-}S)_6(\mu_2\text{-}SH)_6(S_2)_6]^{2-}$ ($\textbf{b-H}_6^{2-}$)

Change in HOMO

Empty Mo d-orbitals   Partially filled Mo d-orbitals

5.1 eV   **HOMO-LUMO Gap**   **2.3 eV**

This journal is © The Royal Society of Chemistry 2025

J. Mater. Chem. A, 2025, **13**, 32382–32390 | **32387**

This observation supports the electronic nature of the PTM observed in XPS and the geometric features observed in d-PDF and XPS. The **b-H$_6^{2-}$** structure has the chemical formula $[Mo^{IV}_7(\mu_3\text{-}S)_6(\mu_2\text{-}SH)_6(S_2)_6]^{2-}$ and comprises six terminal S_2^{2-}, six bridging sulfhydryl (μ_2-SH$^-$), and six (μ_3-S^{2-}) ligands (Fig. 5, right figure). The arrangement and configuration of the main-group elements in this PTM are hence richer than in the parent POM, which only contains oxides.

Discussion

Disulfide and sulfhydryl groups in the PTM geometrically differentiate and contribute to changing the electronic structure of the PTM compared to its parent heptamolybdate cluster. We calculate a HOMO–LUMO gap for the PTM of 2.3 eV, which is much lower than the parent Anderson POM (of 5.1 eV) and consistent with the black color of PTM@NU-1000 crystals. The synthesized PTM consists of seven Mo^{IV} centers, which theoretically requires reduction of 14 electrons to convert all seven Mo^{VI} of the parent POM into Mo^{IV} during synthesis. Conversely, forming the **b-H$_6^{2-}$** cluster involves a two-electron reduction process facilitated as protonation by H$_2$S. This necessitates an additional 12 electron reduction process to explain the PTM's electronic structure observed in XPS. This extra 12 electron reduction process in the **b-H$_6^{2-}$** cluster results from its unique geometric feature of having six terminal disulfides (S_2^{2-}). Terminal disulfides in the PTM structure set it apart from the parent POM structure, which instead has twelve terminal oxides (O^{2-}) while maintaining the similar $Mo_7(\mu_3\text{-S/O})_6(\mu_2\text{-S/O})_6$ core. In the POM, twelve terminal oxides (O^{2-}) carry a total charge of -24, while in the PTM, six terminal disulfides (S_2^{2-}) carry a total charge of -12. This enables the remaining -12 charge to be stabilized by reduction of the molybdenum centers. Frontier molecular orbitals confirm the change in electronic structure accompanying POM to PTM conversion. In the POM, the highest occupied molecular orbital (HOMO) and several orbitals near the HOMO consist of contributions from oxide molecular orbitals, while the d-orbitals of molybdenum are empty due to the Mo^{VI} centers (Fig. 5 and S8). On the other hand, the HOMO, as well as other occupied frontier molecular orbitals near the HOMO of the PTM, have a clear contribution from the partially filled d-orbitals of Mo^{IV} (Fig. 5 and S9).

At the molecular level, the PTM shares geometric and electronic motifs with low-nuclearity thiomolybdate clusters such as $[Mo_3S_{13}]^{2-}$ and $[Mo_2S_{12}]^{2-}$, which are known to contain low-valent Mo centers, short Mo···Mo separations ($\sim$2.7–2.8 Å), and diverse sulfur ligands.[31,32] Simultaneously, the PTM mimics amorphous MoS$_x$ through its short-range atomic order and lack of long-range periodicity, a hallmark of catalytically active amorphous MoS$_x$ phases such as MoS$_3$.[33] However, unlike these bulk amorphous materials, the PTM is atomically precise and chemically uniform, enabling detailed structural modeling and electronic analysis.[4,50]

POM, α-$[Mo^{VI}_7O_{24}]^{6-}$, differs from the parent POM both geometrically and electronically. In contrast to the $[Mo^{VI}_7O_{24}]^{6-}$ cluster, which contains unprotonated oxygen anions exclusively in oxidation state $-$II, the sulfided cluster includes a variety of sulfur anions (S^2, HS$^-$, and S_2^{2-}). Obtained by treating the POM with H$_2$S, the replacement of oxygen by sulfur is complete in the PTM. DFT calculations indicate that H$_2$S works as a reducing agent, converting Mo^{VI} ions to Mo^{IV} while also generating partially oxidized, terminal disulfides (S_2^{2-}, formal oxidation state $-$I). PDF analysis of total X-ray scattering yields key atom–atom separation distances. Combining this structural information with the results of further DFT calculations and with comparisons to modeling results for an extensive collection of candidate PTM structures yields as a best structure of $[Mo^{IV}_7(\mu_3\text{-}S)_6(\mu_2\text{-}SH)_6(S_2)_6]^{2-}$.

Building on this, the POM@MOF to PTM@MOF conversion enables a pivot in catalytic focus away from cluster-enabled oxidation reactions and toward reduction reactions, including hydrogenation and other proton-coupled redox reactions. Preliminary results indicate that catalytic activity emerges only after partial sulfur loss and exposure of metal-ion sites and that the activated form sustains hydrogenation and dehydration at moderate temperatures but deactivates at higher temperatures. Preliminary results also indicate that the as-synthesized and activated materials are susceptible to oxidative degradation upon prolonged air exposure, underscoring the need for inert handling. These current results indicate strong potential for practical gas-phase catalysis with proper activation and protection. Exploration of the generality of MOF-isolation-enabled formation of arrays of stable, agglomeration-resistant PTMs from similarly configured POMs is a focus of current work, as is the catalytic application of reactant-accessible PTMs to energy-science-relevant reduction reactions.

Author contributions

S. M. G. R. performed the DFT modeling and calculations and prepared the original draft. Z. C. conducted the PDF and DED experiments, and J. S. carried out the XPS and ICP-OES measurements. K. W. C. and J. T. H. supervised the experimental work and contributed to manuscript editing. R. B. G. supervised the computational work and contributed to the writing and editing of the manuscript. All authors participated in discussions and data analysis and have approved the final version of the manuscript.

Conflicts of interest

J.T.H. an equity interest in NuMat Technologies, a company that commercializes MOFs. MOFkey is as follows: Zr.HVCDAMXLLUJLQZ.MOFkey-v1.csq (NU-1000).

Conclusions

A combined computational and experimental study shows that a MOF-enshrouded and fully sulfided analog of a representative

Data availability

The data supporting this article have been included as part of the SI. See DOI: **https://doi.org/10.1039/d5ta03649f**.

32388 | *J. Mater. Chem. A*, 2025, **13**, 32382–32390

This journal is © The Royal Society of Chemistry 2025

Acknowledgements

References

1 A. Begum, A. H. Sheikh, G. Moula and S. Sarkar, Fe4S4 cubane type cluster immobilized on a graphene support: a high performance H2 evolution catalysis in acidic water, *Sci. Rep.*, 2017, **7**(1), 16948.

2 R. Weindl, R. Khare, L. Kovarik, A. Jentys, K. Reuter, H. Shi and J. A. Lercher, Zeolite-Stabilized Di-and Tetranuclear Molybdenum Sulfide Clusters Form Stable Catalytic Hydrogenation Sites, *Angew. Chem.*, 2021, **133**(17), 9387–9391.

3 V. Waser, M. Mukherjee, R. Tachibana, N. V. Igareta and T. R. Ward, An artificial [Fe4S4]-containing metalloenzyme for the reduction of CO2 to hydrocarbons, *J. Am. Chem. Soc.*, 2023, **145**(27), 14823–14830.

4 S. Batool, M. Langer, S. N. Myakala, M. Heiland, D. Eder, C. Streb and A. Cherevan, Thiomolybdate Clusters: From Homogeneous Catalysis to Heterogenization and Active Sites, *Adv. Mater.*, 2024, **36**(7), 2305730.

5 J. H. Gillen, C. A. Moore, M. Vuong, J. Shajahan, M. R. Anstey, J. R. Alston and C. M. Bejger, Synthesis and disassembly of an organometallic polymer comprising redox-active Co 4 S 4 clusters and Janus biscarbene linkers, *Chem. Commun.*, 2022, **58**(31), 4885–4888.

6 O. Einsle and D. C. Rees, Structural enzymology of nitrogenase enzymes, *Chem. Rev.*, 2020, **120**(12), 4969–5004.

7 L. C. Seefeldt, Z.-Y. Yang, D. A. Lukoyanov, D. F. Harris, D. R. Dean, S. Raugei and B. M. Hoffman, Reduction of substrates by nitrogenases, *Chem. Rev.*, 2020, **120**(12), 5082–5106.

8 H. L. Rutledge and F. A. Tezcan, Electron transfer in nitrogenase, *Chem. Rev.*, 2020, **120**(12), 5158–5193.

9 I. Moura, J. J. G. Moura, S. R. Pauleta and L. B. Maia, *Metalloenzymes in Denitrification: Applications and Environmental Impacts*, Royal Society of Chemistry, 2016.

10 R. Hille, The mononuclear molybdenum enzymes, *Chem. Rev.*, 1996, **96**(7), 2757–2816.

11 L. B. Maia, I. Moura and J. J. G. Moura, Molybdenum and tungsten-containing enzymes: an overview, in *Molybdenum and Tungsten Enzymes: Biochemistry*, ed. R. Hille, C. Schulzke and M. L. Kirk, The Royal Society of Chemistry, Cambridge, 2016, pp. 1–80.

12 R. Breglia, F. Arrigoni, M. Sensi, C. Greco, P. Fantucci, L. De Gioia and M. Bruschi, First-principles calculations on Ni, Fe-containing carbon monoxide dehydrogenases reveal key stereoelectronic features for binding and release of CO2 to/from the C-cluster, *Inorg. Chem.*, 2020, **60**(1), 387–402.

13 U. Terranova, Residues surrounding the active centre of carbon monoxide dehydrogenase are key in converting CO2 to CO, *JBIC, J. Biol. Inorg. Chem.*, 2021, **26**(5), 617–624.

14 U. Riaz, O. J. Curnow and M. D. Curtis, Desulfurization of organic sulfur compounds mediated by a molybdenum/cobalt/sulfur cluster, *J. Am. Chem. Soc.*, 1994, **116**(10), 4357–4363.

15 M. Wang, L. Zhang, Y. He and H. Zhu, Recent advances in transition-metal-sulfide-based bifunctional electrocatalysts for overall water splitting, *J. Mater. Chem. A*, 2021, **9**(9), 5320–5363.

16 M. D. Curtis, *Hydrodesulfurization Catalysts and Catalyst Models Based on Mo—Co—S Clusters and Exfoliated MoS₂*, ACS Publications, 1996.

17 M. T. Stiebritz, C. J. Hiller, N. S. Sickerman, C. C. Lee, K. Tanifuji, Y. Ohki and Y. Hu, Ambient conversion of CO2 to hydrocarbons by biogenic and synthetic [Fe4S4] clusters, *Nature Catalysis*, 2018, **1**(6), 444–451.

18 M. T. Pope, Y. Jeannin and M. Fournier, *Heteropoly and Isopoly Oxometalates*, Springer, 1983, vol. 33.

19 M. T. Pope and A. Müller, Introduction to polyoxometalate chemistry: from topology *via* self-assembly to applications, in *Polyoxometalate Chemistry from Topology via Self-Assembly to Applications*, Springer, 2001, pp. 1–6.

20 D.-L. Long, E. Burkholder and L. Cronin, Polyoxometalate clusters, nanostructures and materials: From self assembly to designer materials and devices, *Chem. Soc. Rev.*, 2007, **36**(1), 105–121.

21 E. Cadot, M. N. Sokolov, V. P. Fedin, C. Simonnet-Jégat, S. Floquet and F. Sécheresse, A building block strategy to access sulfur-functionalized polyoxometalate based systems using {Mo 2 S 2 O 2} and {Mo 3 S 4} as constitutional units, linkers or templates, *Chem. Soc. Rev.*, 2012, **41**(22), 7335–7353.

22 A. Müller, V. Fedin, K. Hegetschweiler and W. Amrein, Characterization of amorphous substances by studying isotopically labelled compounds with FAB–MS: evidence for extrusion of triangular Mo3IV clusters from a mixture of 92MoS3 and 100MoS3 by reaction with OH⁻, *J. Chem. Soc., Chem. Commun.*, 1992, (24), 1795–1796.

23 P. Braunstein, *Met. Clusters Chem.*, 1999, **1**, 1.

24 T. Shibahara, Syntheses of sulphur-bridged molybdenum and tungsten coordination compounds, *Coord. Chem. Rev.*, 1993, **123**(1–2), 73–147.

25 B. J. Bucior, A. S. Rosen, M. Haranczyk, Z. Yao, M. E. Ziebel, O. K. Farha, J. T. Hupp, J. I. Siepmann, A. Aspuru-Guzik and R. Q. Snurr, Identification schemes for metal–organic frameworks to enable rapid search and cheminformatics analysis, *Cryst. Growth Des.*, 2019, **19**(11), 6682–6697.

26 J. E. Mondloch, W. Bury, D. Fairen-Jimenez, S. Kwon, E. J. DeMarco, M. H. Weston, A. A. Sarjeant, S. T. Nguyen, P. C. Stair and R. Q. Snurr, Vapor-phase metalation by

This journal is © The Royal Society of Chemistry 2025

J. Mater. Chem. A, 2025, **13**, 32382–32390 | **32389**

atomic layer deposition in a metal–organic framework, *J. Am. Chem. Soc.*, 2013, **135**(28), 10294–10297.

27 J. Duan, H. Shabbir, Z. Chen, W. Bi, Q. Liu, J. Sui, L. Đorđević, S. I. Stupp, K. W. Chapman and A. B. F. Martinson, Synthetic access to a framework-stabilized and fully sulfided analogue of an Anderson polyoxometalate that is catalytically competent for reduction reactions, *J. Am. Chem. Soc.*, 2023, **145**(13), 7268–7277.

28 T. F. Jaramillo, K. P. Jørgensen, J. Bonde, J. H. Nielsen, S. Horch and I. Chorkendorff, Identification of active edge sites for electrochemical H2 evolution from MoS2 nanocatalysts, *Science*, 2007, **317**(5834), 100–102.

29 Y. Li, H. Wang, L. Xie, Y. Liang, G. Hong and H. Dai, MoS2 nanoparticles grown on graphene: an advanced catalyst for the hydrogen evolution reaction, *J. Am. Chem. Soc.*, 2011, **133**(19), 7296–7299.

30 K. Chang, Z. Mei, T. Wang, Q. Kang, S. Ouyang and J. Ye, MoS2/graphene cocatalyst for efficient photocatalytic H2 evolution under visible light irradiation, *ACS Nano*, 2014, **8**(7), 7078–7087.

31 J. Kibsgaard, T. F. Jaramillo and F. Besenbacher, Building an appropriate active-site motif into a hydrogen-evolution catalyst with thiomolybdate [Mo3S13] 2− clusters, *Nat. Chem.*, 2014, **6**(3), 248–253.

32 Z. Huang, W. Luo, L. Ma, M. Yu, X. Ren, M. He, S. Polen, K. Click, B. Garrett and J. Lu, Dimeric [Mo2S12] 2− cluster: a molecular analogue of MoS2 edges for superior hydrogen-evolution electrocatalysis, *Angew. Chem., Int. Ed.*, 2015, **54**(50), 15181–15185.

33 C. G. Morales-Guio and X. Hu, Amorphous molybdenum sulfides as hydrogen evolution catalysts, *Acc. Chem. Res.*, 2014, **47**(8), 2671–2681.

34 F. Gonell, M. Rodenes, S. Martín, M. Boronat, I. Sorribes and A. Corma, From Well-Defined Clusters to Functional Materials: Molecular Engineering of Amorphous Molybdenum Sulfides for Hydrogen Evolution Electrocatalysis, *Chem. Mater.*, 2023, **35**(20), 8483–8493.

35 P. D. Tran, T. V. Tran, M. Orio, S. Torelli, Q. D. Truong, K. Nayuki, Y. Sasaki, S. Y. Chiam, R. Yi and I. Honma, Coordination polymer structure and revisited hydrogen evolution catalytic mechanism for amorphous molybdenum sulfide, *Nat. Mater.*, 2016, **15**(6), 640–646.

36 T. E. Webber, W.-G. Liu, S. P. Desai, C. C. Lu, D. G. Truhlar and R. L. Penn, Role of a Modulator in the Synthesis of Phase-Pure NU-1000, *ACS Appl. Mater. Interfaces*, 2017, **9**(45), 39342–39346.

37 M. J. Frisch, G. W. Trucks, H. B. Schlegel, G. E. Scuseria, M. A. Robb, J. R. Cheeseman, G. Scalmani, V. Barone, G. A. Petersson and H. Nakatsuji, *Gaussian 16, Revision a. 03*, Gaussian, Inc., Wallingford, 2016.

38 Y. Zhao and D. G. Truhlar, A new local density functional for main-group thermochemistry, transition metal bonding, thermochemical kinetics, and noncovalent interactions, *J. Chem. Phys.*, 2006, **125**(19), 194101.

39 F. Weigend and R. Ahlrichs, Balanced basis sets of split valence, triple zeta valence and quadruple zeta valence quality for H to Rn: Design and assessment of accuracy, *Phys. Chem. Chem. Phys.*, 2005, **7**(18), 3297–3305.

40 F. Weigend, Accurate Coulomb-fitting basis sets for H to Rn, *Phys. Chem. Chem. Phys.*, 2006, **8**(9), 1057–1065.

41 A. V. Marenich, C. J. Cramer and D. G. Truhlar, Universal solvation model based on solute electron density and on a continuum model of the solvent defined by the bulk dielectric constant and atomic surface tensions, *J. Phys. Chem. B*, 2009, **113**(18), 6378–6396.

42 S. Y. Haoyu, X. He, S. L. Li and D. G. Truhlar, MN15: A Kohn–Sham global-hybrid exchange–correlation density functional with broad accuracy for multi-reference and single-reference systems and noncovalent interactions, *Chem. Sci.*, 2016, **7**(8), 5032–5051.

43 Y. Huang, Y. Sun, X. Zheng, T. Aoki, B. Pattengale, J. Huang, X. He, W. Bian, S. Younan and N. Williams, Atomically engineering activation sites onto metallic 1T-MoS2 catalysts for enhanced electrochemical hydrogen evolution, *Nat. Commun.*, 2019, **10**(1), 982.

44 A. E. Platero-Prats, A. B. League, V. Bernales, J. Ye, L. C. Gallington, A. Vjunov, N. M. Schweitzer, Z. Li, J. Zheng and B. L. Mehdi, Bridging zirconia nodes within a metal–organic framework *via* catalytic Ni-hydroxo clusters to form heterobimetallic nanowires, *J. Am. Chem. Soc.*, 2017, **139**(30), 10410–10418.

45 A. E. Platero-Prats, Z. Li, L. C. Gallington, A. W. Peters, J. T. Hupp, O. K. Farha and K. W. Chapman, Addressing the characterisation challenge to understand catalysis in MOFs: the case of nanoscale Cu supported in NU-1000, *Faraday Discuss.*, 2017, **201**, 337–350.

46 K. Wang, W. Hua, Z. Li, Q. Wang, C. Kübel and X. Mu, New insight into desodiation/sodiation mechanism of MoS2: Sodium insertion in amorphous Mo–S clusters, *ACS Appl. Mater. Interfaces*, 2021, **13**(34), 40481–40488.

47 A. Müller, S. Sarkar, R. G. Bhattacharyya, S. Pohl and M. Dartmann, Directed synthesis of [Mo3S13]2−, an isolated cluster containing sulfur atoms in three different states of bonding, *Angew Chem. Int. Ed. Engl.*, 1978, **17**(7), 535.

48 A. Müller, W. O. Nolte and B. Krebs, [(S2) 2Mo (S2) 2Mo (S2) 2] 2−, ein neuartiger Komplex mit nur S-Liganden und einer Mo– Mo-Bindung, *Angew. Chem.*, 1978, **90**(4), 286–287.

49 T. Shibahara and H. Kuroya, Preparation of trinuclear molybdenum (IV) ion, Mo3S4+ 4, and x-ray structure of Ca [Mo3S4 {HN (CH2CO2) 2} 3]· 11.5 H2O, *Polyhedron*, 1986, **5**(1–2), 357–361.

50 S. Batool, S. P. Nandan, S. N. Myakala, A. Rajagopal, J. S. Schubert, P. Ayala, S. Naghdi, H. Saito, J. Bernardi and C. Streb, Surface anchoring and active sites of [Mo3S13] 2– clusters as co-catalysts for photocatalytic hydrogen evolution, *ACS Catal.*, 2022, **12**(11), 6641–6650.

32390 | *J. Mater. Chem. A*, 2025, **13**, 32382–32390

This journal is © The Royal Society of Chemistry 2025